The effect of photoactivated transformations of Ag⁺ and Ag⁰ in silica fillers on their biocidal activity

V. M. Bogatyrov[1] · V. M. Gun'ko[1] · M. V. Galaburda[1] · O. I. Oranska[1] ·
I. S. Petryk[1] · K. S. Tsyganenko[1] · Ya. I. Savchuk[2] · A. Yu. Chobotarov[2] ·
T. V. Rudenchyk[3] · R. A. Rozhnova[3] · N. A. Galatenko[3]

Abstract

Ag and AgCu containing powdered silica fillers of polymers for medical applications have been synthesized using mechanochemical activation with a low content of solvent or dry powdered materials. The samples in the form of filled polymer films were obtained using polyurethane-urea and silica nanocomposites. The composites have been investigated by TEM, UV/Vis spectroscopy, XRD and microbiological analysis. It has been found that amorphous and nanosized structures of silver oxides and metallic Ag nanocrystallites are formed during thermal destruction of silver nitrate or ammonium complexes in silica matrix (fumed or precipitated silica). Sunlight exposure of nanocomposites contained Ag^+ ions leads to the formation of Ag^0 nanocrystallites. After UV irradiation, the decrease in surface plasmon resonance band intensity can be caused by the oxidation of Ag^0. It is found that silica nanocomposites with the low Ag content (0.2 mmol g^{-1} SiO_2) exhibited the highest antimicrobial activity, whereas the polymeric film with a filler content of 1 wt% exhibited the most efficient antimicrobial properties among tested polymeric composites. The observed transformations ($Ag^+ \leftrightarrow Ag^0$) of silver compounds do not suppress the biocidal activity of nanocomposites.

✉ M. V. Galaburda
    mariia.galaburda@gmail.com

[1] Chuiko Institute of Surface Chemistry, 17 General Naumov Street, Kiev 03164, Ukraine

[2] Zabolotny Institute of Microbiology and Virology, 154 Academic Zabolotny Street, Kiev 03143, Ukraine

[3] Institute of Macromolecular Chemistry, 48 Kharkivske Highway, Kiev 02160, Ukraine

Introduction

Biological properties and application features of nanostructured or nanosized particles of metals and their oxides are of importance for both theoretical and practical points of view [1–4]. The materials containing silver nanoparticles are especially interesting due to their high biocidal properties and low toxicity [5–7]. Additionally, the nanocomposites of silver and metal oxide such as titanium, copper, zinc, zirconium or iron oxides are characterized by enhanced biocidal properties, improved photodegradation efficiency of adsorbed microorganisms and self-cleaning ability [8–13]. The nanocomposites consisting of silver nanoparticles and silica are the most studied. Various methods have been applied to obtain the Ag containing silica systems using $AgNO_3$ as a precursor. Silver reduction to metallic particles occurred in an aqueous solution of $NaBH_4$, hydrazine, ascorbic acid, citrates, etc. in the presence of stabilizers, such as amines, amides, sucrose, and polyvinylpyrrolidone. Silica matrix can be prepared by sol–gel technique using tetraethoxysilane as a precursor [14–18]. Core–shell nanomaterials with silica cores can be synthesized using Shtober microspheres [19–21]. In this case, Ag nanoparticles decorate the silica surface forming a mosaic cover. Some silver compounds (deposited onto silica particles) can exhibit the biocidal properties. For example, polymer composites contained silver chloride bound to mesoporous silica exhibited efficient antimicrobial properties [22] as well as Ag_3PO_4 nanoparticles used to intercalate bentonite [23].

To diminish the amount of solvents used in the sol–gel method, an adsorption layer of silica can be applied as a nanoreactor to synthesize silver nanoparticles [24]. This method allows controlling the size distribution of particles due to the confined space effects for growth of crystalline or amorphous nanoparticles (metallic silver or mixture of silver and copper oxides) in relatively narrow pores or interparticle voids. The preparation of Ag–Cu metal alloy nanoparticles using solvothermal method is described elsewhere [25]. However, this method is more complex than mechanochemical; moreover, the formation of huge size particles (100–600 nm) was obtained [25].

From a practical point of view, it is of interest to provide the bactericidal properties for industrial dispersive silica that can simplify production of fillers for polymeric materials with the antimicrobial properties. There are two main methods of industrial production of highly dispersive silica such as sedimentation from silicate solutions and high-temperature oxidation of tetrachloride silicon or methylsilanes (pyrogenic silica). Since the diameter of primary particles of pyrogenic silica and precipitated silica is in the range of 4–40 and 20–50 nm, respectively, with bulk density of 50–200 g L^{-1} for both powders, these materials are considered as nanosilica.

There are several textural and morphological factors of nanosilicas promoting the nanoreactor synthesis of nanoparticles. The specific surface area of the nanosilica is in the range of 50–500 m^2/g that corresponds to 50–5 nm in average diameter of nanoparticles, respectively, forming aggregates and agglomerates of aggregates with a broad size distribution of voids between nanoparticles.

The content of surface OH groups as the main adsorption sites is in the range of 0.25–0.7 mmol/g of SiO$_2$. These factors create favourable conditions for synthesis of nanostructured particles (e.g. Ag) using the nanoreactor method. Mechanochemical method (with a ball-mill) of dispersive silica modification is one of the simplest and environment-friendly method as the used amount of solvents is minimal. This method is effective to produce Ag-containing silica nanocomposites with the bactericidal properties for industrial production as well [26].

In the present work, the dispersive silica modified with silver compounds is used as an antimicrobial filler of polymers for medical applications. During polymer production process, silica filler may be exposed to sunlight or/and UV radiation for material sterilization. Therefore, the influence of sunlight and UV irradiation on antimicrobial activity of Ag containing silica nanocomposites is analysed in this work. Two series of composites have been obtained: the first was obtained by chemical modification of precipitated silica, and the second was based on fumed silica brand of A-300. Both series consist of Ag-(Ag–SiO$_2$) and bimetallic Ag/Cu containing (AgCu–SiO$_2$) silica nanocomposites. The enhanced biocidal activity of the bimetallic AgCu–SiO$_2$ compounds was discussed previously [27]. Composites with precipitated silica were used to prepare antimicrobial polymeric materials while composites with fumed silica were used for assessment of the impact of sunlight and ultraviolet irradiation on the antimicrobial activity of the compounds.

Materials and methods

Reagents

Fumed silica brand of A-300 (Pilot plant of Chuiko Institute of Surface Chemistry, Kalush, Ukraine) and precipitated silica NewSil-125 (China) have been used as silica matrices. To modify silica, AgNO$_3$, Cu(CH$_3$COO)$_2$·H$_2$O (CuAc$_2$·H$_2$O), 25% aqueous ammonia solution and distilled water were used. The synthesis of

Table 1 Content of components used for the synthesis of biocidal fillers (silica amount was constant 50 g)

Samples	AgNO$_3$ (g)	CuAc$_2$·H$_2$O (g)	NH$_4$OH (g)	H$_2$O (g)	Thermal treatment (°C)	Duration of thermal treatment (h)
01Ag-P	0.85	–	4.00	11.27	200	2.0
01Ag02Cu-P	0.85	1.96	11.00	5.14	200	2.0
02Ag02Cu-P	1.70	1.99	14.52	0.50	200	2.0
02Ag-F	1.70	–	8.00	45.70	350	1.5
02Ag02Cu-F	1.71	2.00	31.94	24.30	350	1.5
1Ag-F	8.5	–	–	10.00	450	1.5

The amount of metals was 0.1, 0.2 and 1 mmol per 1 g of silica (it corresponds to sample labels with 01, 02 and 1, respectively). Samples with precipitated and fumed silica are labelled as "P" and "F", respectively

nanocomposites was carried out by mechanochemical activation with a porcelain ball mill (2 L in volume) using various amounts of components (Table 1). The prepared white or bluish (in the presence of copper) powders were heated in air at 200–450 °C for 1.5–2 h.

During matrix modification, the formation of $[Ag(NH_3)_2]^+$ and $[Cu(NH_3)_4]^{2+}$ on a silica surface took place as a result of metal salt dissolution in ammonia solution. Deposition of silver from ammonia complexes is the preferred way as their thermal destruction takes place at relative low temperature (near 100 °C) [28, 29] compared to copper acetate and silver nitrate (above 450 °C). Further increase of the temperature brings to silver oxide and Ag^0 formation in silica composites. Variation of the ammonia/water ratio was determined by the required amount of ammonia for the formation of ammonia complexes ($[Ag(NH_3)_2]^+$ and $[Cu(NH_3)]^{2+}$) maintaining the ratio of dry silica/liquid for each series of samples (Table 1). The number in the sample's abbreviation means the content of the metals in the composites (mmol/g of silica). 1Ag-F composite was used as a reference sample with the highest content of Ag nanoparticles.

Materials based on polyurethane-urea (PUU) have been used for creation of film coverage for wound treatment, as well as catheters, vessels, etc. The antibacterial properties of these materials can be provided by filling with silver nanoparticles [30]. In this work, the hydrophilic polymer was synthesized using PUU with the following copolymers: N-vinylpyrrolidone, vinyl acetate with vinyl alcohol, according to the procedure described elsewhere [31]. The composites with modified silica (1 wt%) were prepared by mechanical mixing with polymer solution at room temperature with the following degassing to remove air from polymer composites. The polymeric solutions were dried on Teflon substrates at 60 °C for several days for formation of elastic and strong films with thickness of 0.2–0.3 mm. During the synthesis, some other compounds have also been used: polyoxypropyleneglycol (Rokopol, Poland) dried at 80 ± 5 °C and 0.001–0.004 atm in dry argon flow for 8 h; 2.4-; 2.6-toluylene diisocyanate (80/20) $C_9H_6N_2O_2$ (Merck, Germany); 4.4′-diaminodiphenylmethane $C_{13}H_{14}N_2$ (Fluka, 97.0%); and N,N'-dimethylacetamide (Merck, Germany). Co-polymer of N-vinylpyrrolidone, vinyl-acetic ester, and vinyl alcohol (Sigma-Aldrich) were synthesized using basic alcoholysis with incomplete saponification.

Instruments and measurements

Transmission electronic microscopy a JEM-1400 (Jeol, Japan) was used at the accelerating voltage of 80 kV. Samples of silica composites were dispersed in distilled water. A drop of a suspension was place onto a copper grid with a cove. The samples were dried in air at room temperature. For the 1Ag-F sample, a JEM-2100F was used with a X-ray microanalyzer (Oxford).

The UV/Vis spectra (transmission mode for polymeric films and diffuse reflectance mode for silica powders) were recorded using a UV/Vis Lambda 35 spectrophotometer (Perkin Elmer). The Kubelka–Munk function $F(hv)$ obtained from the equation

$F(hv) = (1-R(hv))^2/(2R(hv))$, where $R(hv)$ is the diffuse reflectance data, is proportional to absorbance.

X-ray diffraction (XRD) patterns were recorded over $2\theta = 10–80°$ range using a DRON-4-07 (Burevestnik, St. Petersburg) diffractometer with CuK ($\lambda = 0.15418$ nm) irradiation and a Ni filter. To investigate the structural properties of composites under sunlight exposure, the sample was permanently pressed into a quartz holder and placed in ambient lighting conditions in a laboratory room. The sunlight exposure was tested for 1–30 days using daylight in the laboratory room during August–September. For UV radiation, a fluorescent bactericidal lamp T8 30W G13 (253.7 nm, China) was used. All samples were irradiated in Petri dishes.

Microbiological study

The test microorganisms were received from American Type Culture Collection and *National Collection of Type Cultures (*Public Health England*)*. The antimicrobial activity was determined using pharmacopoeia strains of Gram-positive bacteria *Bacillus subtilis* ATCC 6633, *Staphylococcus aureus* ATCC 6538, *S. epidermidis* ATCC 12228, *Micrococcus flavus* ATCC 10240, Gram-negative bacteria *Pseudomonas aeruginosa* ATCC 9027, *Escherichia coli* ATCC 25922, *Salmonella enteric* NCTC 6017, *Proteus vulgaris* ATCC 6896, and yeast-like fungus *Candida albicans* ATCC 10231. Test microorganisms were grown on nutrient agar (HiMedia Laboratories Pvt. Ltd., India).

The antimicrobial activity was defined by agar disc diffusion [32]. Agar plates were inoculated with the test microorganism with final a size of 0.5 McFarland, which corresponds $(1–2) \times 10^8$ CFU/mL for bacteria and $(1–5) \times 10^6$ CFU/mL for yeasts. The examined polymeric composite discs with a diameter of 8 mm were placed on the agar surfaces and were incubated at a temperature of 35 ± 2 °C for 18 h. Then, the diameters of inhibition growth zosne were measured. The antimicrobial activity of processed silica fillers was defined by agar well diffusion method [32]. Agar plates and test organisms were prepared similarly to the agar disc diffusion method. Then, a hole with a diameter of 8 mm was punched with a sterile cork-borer, and 20 mg of the each examined samples were introduced into the wells. Additionally, the diameters of inhibition growth zones were measured after incubation for 18 h. The significance of bacterial growth retardation zones relative to different parameters was examined by two-way ANOVA test. Irradiation was considered to have a significant effect on the results when the p value was less than 0.01 (99% confidence level). All experiments were performed four times and are represented as mean $\pm$ SD. The average values of four replicates (0—no activity; $p < 0.01$) were used.

Results and discussion

Synthesis of Ag containing composites using precipitated silica and investigation of antimicrobial properties of filled polymeric materials

All silica nanocomposites were obtained using mechanochemical approach. The composites (Table 1) were represented as powders sieved with 0.5 mm mesh. The appearance of a surface plasmon resonance (SPR) band at 405–450 nm in UV/Vis spectra (Fig. 1) is noted for the samples containing silver. It should be noted that the synthesis conditions of Ag containing silica systems significantly affect the shape of the spectrum and the position of the absorption bands of the UV/Vis spectra as a result of the different size and shape of silver and silica nanoparticles as well as the nature of silver compounds formed during the synthesis using various methods [33–35]. Depending on the mentioned factors, the surface plasmon resonance band can be broadened and shifted toward 650 nm [33]. In the presence of copper, a broad band can be observed at 700–800 nm pointing on copper oxides bound on the silica surface and belongs to d–d transitions in Cu^{2+} ions in octahedral environment [36]. Additional explanation on the spectral characteristics of silica modified with silver and copper compounds, as well as the SPR shift is discussed in detail in the next section.

Figure 2 shows the TEM images and the particle size distribution of the samples with precipitated silica. The presence of copper ions and changes in the reaction environment affect the size distribution of metal particles. It has to be emphasised that the decrease of the silver particle size has been noted for the composites contained both silver and copper at silica surface that is also consistent with the results of the work of Jiang et al. [37]. It should be pointed out that the impact of sunlight exposure during the synthesis of the first series of silica samples and filled polymer was not controlled.
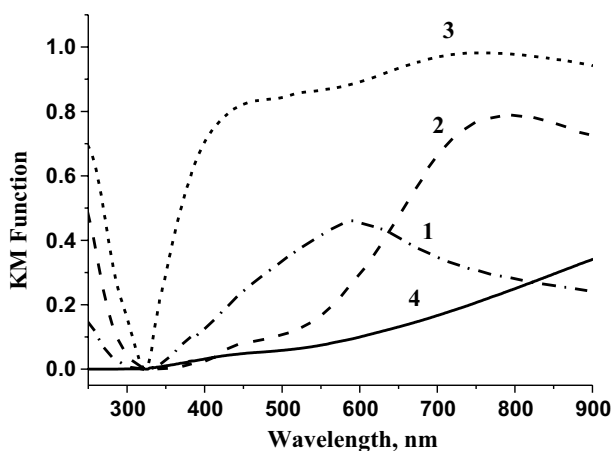

Fig. 1 UV/Vis spectra of 01Ag-P (1), 01Ag02Cu-P (2), 02Ag02Cu-P (3) and bare precipitated silica (4) composites
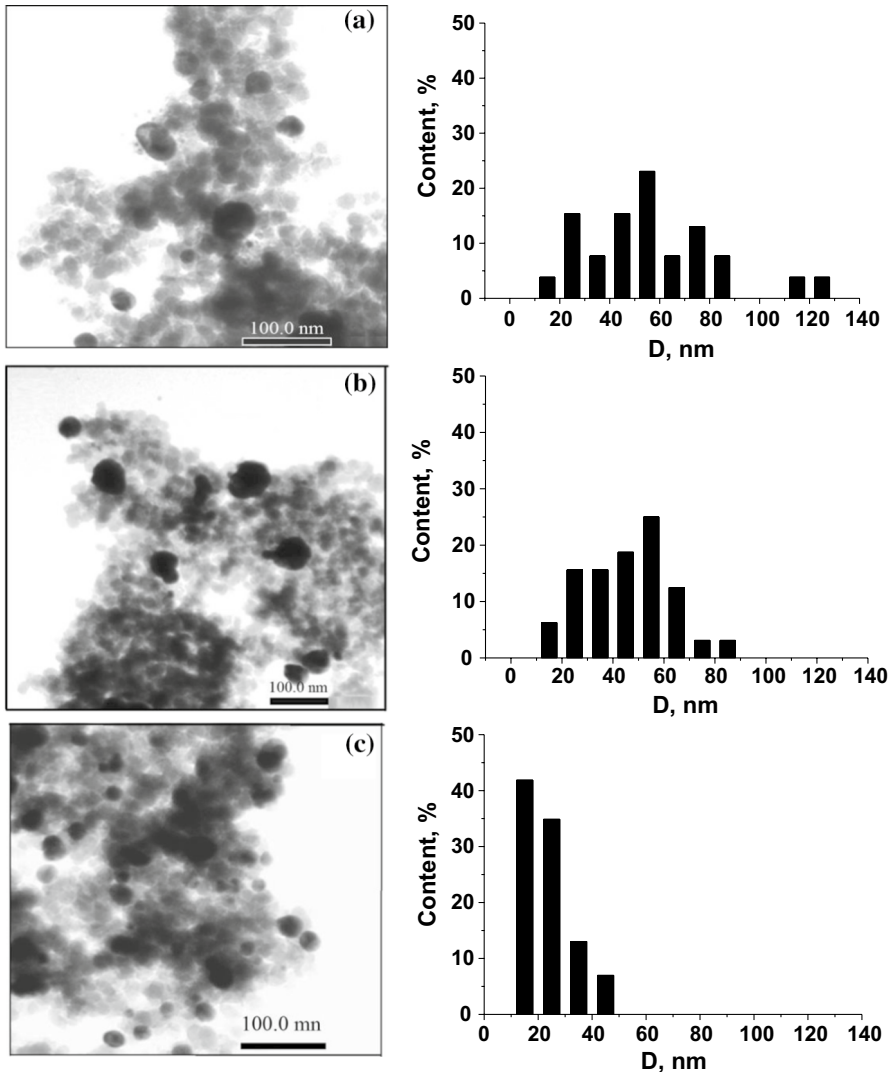
Fig. 2 TEM images and related particle size distributions of metal nanoparticles for samples: 01Ag-P (**a**), 01Ag02Cu-P (**b**) and 02Ag02Cu-P (**c**)

UV/Vis absorption spectra of the polymer films filled with the composites are shown in Fig. 3. The observed maxima in the region of 437–445 nm is related to Ag SPR band (Fig. 3). As known, the shape of SPR band are different for powdered composites because SPR absorption is sensitive not only to geometric parameters, microstructure and aggregated structure of nanoparticles but also to the surrounding matrix. Interfacial physical or chemical interaction may induce changes in the electronic band structure and optical interband transitions of the particle surface as well as deviations of dielectric properties of nanoparticle/
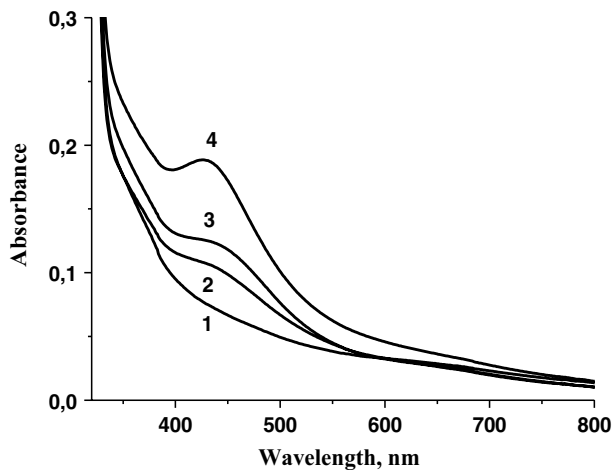
Fig. 3 Absorption spectra of the initial polymer (1), the polymeric films filled with 01Ag-P (2), 01Ag02Cu-P (3) and 02Ag02Cu-P (4) nanocomposites

matrix interlayers from the bulk polymer [33–35, 38]. The spectral characteristics of the films and silica powders were obtained from transmittance and diffuse reflection spectra, respectively, taking into account that the polymer film contains only 1 wt% of modified silica filler. During synthesis procedure of polyurethane-urea polymer with modified silica filler, chemical transformations of the surface silver ($Ag^+ \rightarrow Ag^0$) and copper ions can occur. The structure of silver and copper compounds in silica filler is discussed in detail in the next section. All possible chemical transformations of silver and copper compounds under the action of the functional groups of polymer components require the detailed research in each specific case of creating a new polymer composite.

The position of the SPR band can also be affected by a change in the molecular environment and the aggregation level of silver nanoparticles due to the adsorption of monomers on the surface of silver nanoparticles during the synthesis of a polymer composite. The reduction of Ag^+ to Ag^0 in the doped silica nanoparticles in the polymer matrices can also affect its offset.

The antimicrobial activity of the polymer composites filled with modified silica (1 wt%) was investigated against both Gram-negative and Gram-positive bacteria (Fig. 4, Table 2).

The difference in diameter of the inhibition zones can be connected with the most effective inhibitory activity against both Gram-negative and Gram-positive bacteria of the polymer doped with 02Ag02Cu-P nanoparticles (the inhibition zones without bacterial growth are distinctly visible). Unmodified NewSil-125 was used as a blank test to confirm that metal nanoparticles rather than silica or other species caused the observed growth inhibition.
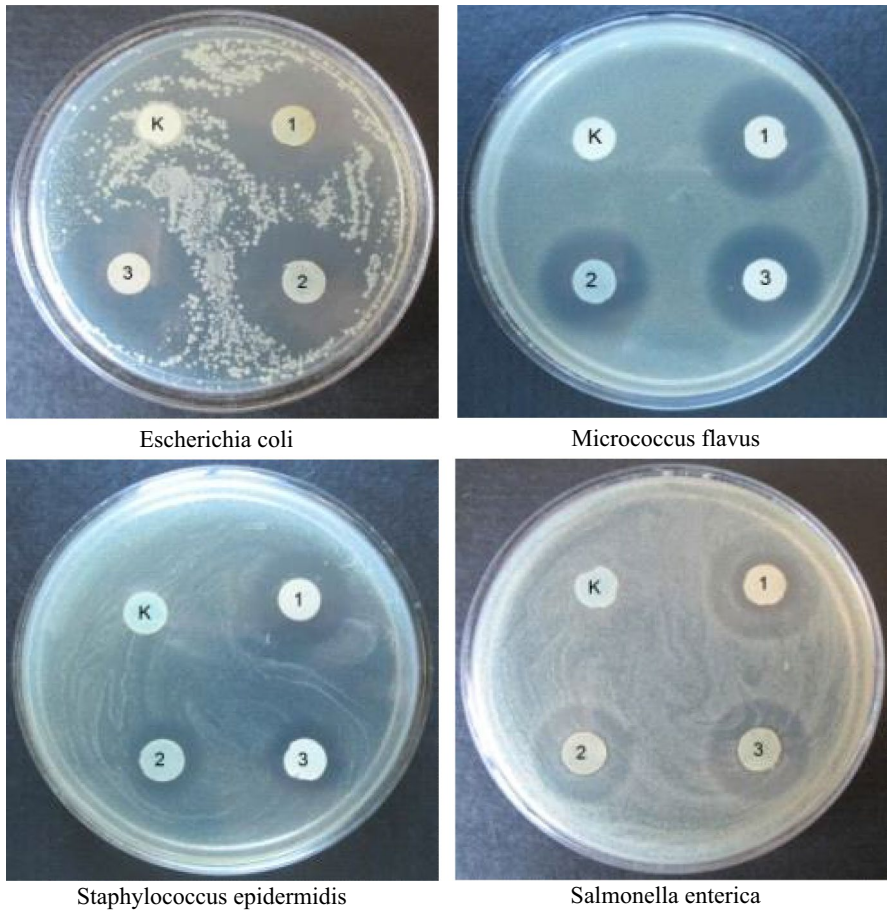
Escherichia coli

Micrococcus flavus

Staphylococcus epidermidis

Salmonella enterica

Fig. 4 Growth delay zones for polymers with 02Ag02Cu-P (1), 01Ag02Cu-P (2), 01Ag-P (3) and NewSil-125 (K)

Table 2 Growth delay zones (in mm) of microorganisms on polymers with silica nanocomposites

Bacterial culture	01Ag-P	01Ag02Cu-P	02Ag02Cu-P	NewSil-125 control
Pseudomonas aeruginosa	14	13	20	0
Escherichia coli	27	27	30	0
Salmonella enterica	24	23	28	0
Proteus vulgaris	31	30	31	0
Bacillus subtilis	19	22	25	0
Staphylococcus aureus	18	18	21	0
Salmonella epidermidis	18	20	27	0
Micrococcus flavus	25	25	29	0

The table shows the average value of four replicates; 0—no activity; $p < 0.01$

Synthesis of Ag containing composites based on fumed silica and investigation of the impact of sunlight exposure and ultraviolet radiation on the antimicrobial activity

To understand and control the properties of composites, the synthesis of Ag containing silica composites need to be taken into consideration. During the synthesis, chemical reagents for reduction of Ag^+ to Ag^0 were not used. The formation of Ag^0 took place upon thermal decomposition of silver nitrate according to the scheme:

$$2AgNO_3 \xrightarrow{T\,°C} 2Ag + NO_2 + NO + 1.5O_2 \tag{1.1}$$
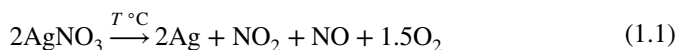
Decomposition of silver nitrate (1.1) is started at $T > 360$ °C and finished at 515 °C according to the thermogravimetric data [39]. Ag_2O can be formed as an intermediate in this process regardless of the oxidizing or inert atmosphere. The formation of silver oxides from precipitated $AgNO_3$ on the surface of SiO_2 nanoparticles after heating at 450 °C in air was previously established [26]. The obtained value of interplanar distances from the TEM image confirms the presence of the silver oxide phase in 1Ag-F nanocomposite. A region with an ordered structure and dimensions of interplanar distances characteristic for silver oxide is observed (Fig. 5a). The micrograph shows the periodicity of the particle planes of 0.24–0.26 nm which is comparable with interplanar distances of silver oxides, such as, for example, $d_{(200)}$ AgO (ICDD 76-1489), $d_{(002)}$ Ag_2O (ICDD 72-2108), $d_{(200)}$ Ag_2O_3 (ICDD 72-607), $d_{(111)}$ Ag_3O_4 (ICDD 77-1846).

The TEM image (Fig. 5b) indicates the formation of the separated particles, namely Ag^0, which is confirmed by elemental analysis. The route of the silver nanoparticles formation can occur through the appearance og Si–O–metal bonds as a result of the interaction of surface OH groups of silica surface with silver species as described in [26]. They are destroyed by heat treatment in air atmosphere in the presence of water vapour with further formation of metal oxides and Si–OH groups. The obtained silver oxides have independent antimicrobial activity and are an intermediate compound in the further formation of Ag^0 nanoparticles. Silver
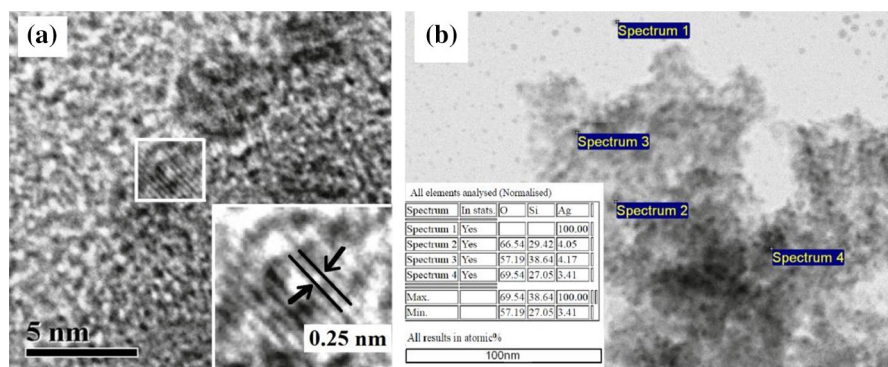

Fig. 5 TEM images of 1Ag-F nanocomposite

nanoparticles are spatially separated in highly dispersive silica and do not have strong chemical bonds with the matrix. Nevertheless, spatial separation of metal nanoparticles in silica composites that prevents their agglomeration as well as the presence of surface oxide layer of the silver nanoparticles, which prevents their oxidation by atmospheric oxygen in the absence of active chemical reagents [40], leads to high nanoparticle stability over time. However, taking into consideration that the sample preparation for TEM study was carried out using ultrasonic treatment, Ag nanoparticles can be removed from the silica surface during this process.

The structural changes of 1Ag-F sample as a function of sunlight exposure was analysed by XRD method. Before sunlight exposure, the wide low-intensive peaks in the region of silver and silver oxides on the XRD patterns of 1Ag-F sample (Fig. 6, curve 1) are observed. It can be related to the beginning of the formation of crystal structures and a small number of formed nanocrystallites of oxide and metal particles in silica matrix. During daily measurements (for 30 days), it was experimentally established that the crystallites of silver were formed after 8 days of sunlight exposure (Fig. 6, curve 3).

In contrast to silver nitrate decomposition, the thermal decomposition of $[Ag(NH_3)_2]^+$ complexes occurs at much lower temperatures. This route was used to prepare Ag containing composites based on Silochrome S-120 via thermal decomposition of the adsorbed complexes at 200 °C [28]. Thermal decomposition of the ammonia complex also proceeds through the formation of Ag_2O.

The effects of sunlight and UV irradiation on transformation of silver compounds in silica nanocomposites were analysed for 02Ag-F and 02Ag02Cu-F (Figs. 7 and 8). It should be noted that the synthesized samples were stored in dark glass bottles to avoid contact with sunlight.

The broad low-intensive SPR band with a maximum at 403 nm is observed in the spectrum of initial 02Ag-F sample (before irradiation) (Fig. 7, curve 2), which corresponds to silver nanoparticles formation. After exposure to sunlight during
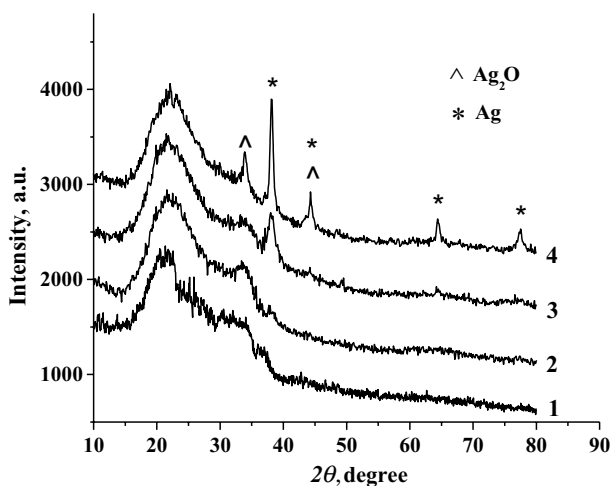

Fig. 6 XRD patterns of 1Ag-F before (1) and after sunlight exposure for 3 (2), 8 (3), and 30 (4) days
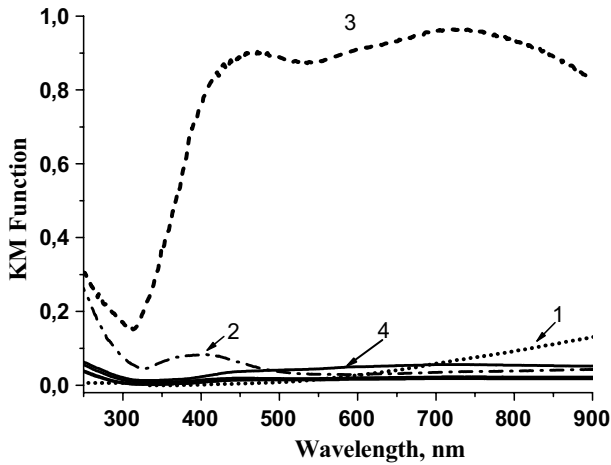
Fig. 7 UV/Vis spectra of silica (1), 02Ag-F sample before (2), after sunlight exposure for 10 days (3) and UV irradiation for 30 (4), 60, 90 and 120 min (other solid lines)
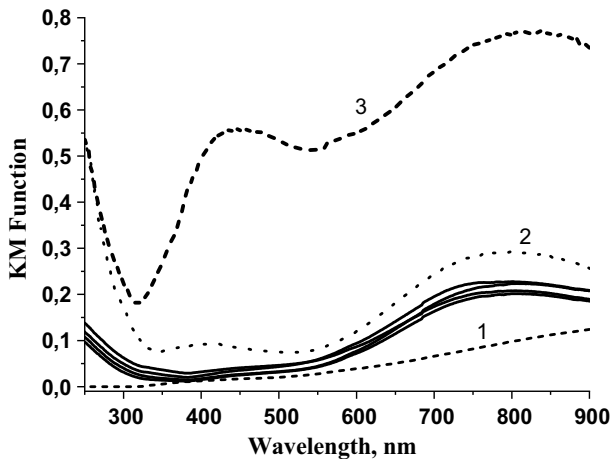

Fig. 8 UV/Vis spectra of silica (1), 02Ag02Cu-F samples before (2), after sunlight exposure for 10 days (3) and UV irradiation for 30, 60, 90 and 120 min (solid lines)

10 days, the intensity of the SPR band is significantly increased and the position of the maximum shifts to 464 nm. At the same time, a wide absorption band appears with a maximum in the region of 725 nm (Fig. 7, curve 3), which can be attributed to the formation of AgNPs of different size and shapes as reported herein [41]. In the case of UV irradiation of the initial 02Ag-F sample, the disappearance of the SPR band at 403 nm observed for this sample (Fig. 7, curve 2) takes place after UV exposure for 30 min with the following slight decrease in the absorption intensity up to 120 min of irradiation (Fig. 7, solid lines).

The bimetallic silica nanocomposites were synthesized via chemical modification of the silica surface with ammonia complexes of metals with subsequent thermal treatment and formation of $Cu(OH)_2$, CuO, Ag_2O, and Ag^0 particles [28]. The content of copper compounds in the composites was very low (0.2 mmol/g SiO_2), which did not even allow the formation of a uniform monolayer on the surface of silica particles; therefore, it was impossible to get any useful information from TEM and XRD investigation. The presence of copper species can be identified by UV/Vis spectroscopy (Figs. 1 and 8) through the appearance of absorption band in the region of 700–800 nm that is characteristic to d–d transitions of dispersive Cu^{2+} species [36]. The UV/Vis spectra of 02Ag02Cu-F sample after sunlight irradiation (Fig. 8, curve 3) can be deconvoluted into three Gaussian components with maxima at 420, 498 and 787 nm at $R^2 = 0.982$ (not shown here). These deconvoluted peaks correspond to SPR bands of AgNPs and CuO particles. Apart from that, Cardoso-Avila et al. [41] reported that the absorption bands of irradiated AgNPs by blue and green light appeared in the range of 400–700 nm were caused by the changes in the shape and size of the particles. It follows that the spectral characteristics of silica modified with silver and copper demonstrate the appearance of SPR band in the region of 400–420 nm and the broad absorption at longer wavelengths belong to AgNPs (spheres) and AgNPs (triangles, rods etc.) along with copper species, respectively, and point that the shape of the nanoparticles depends on the photoactivation conditions of the nanocomposite.

In the spectrum of the initial 02Ag02Cu-F sample, the SPR band at 412 nm signed to AgNPs and an absorption band in the region of 790 nm attributed to copper oxide (CuO) are observed (Fig. 8, curve 2). After daylight exposure, the intensity of both SPR and long-wavelength absorption bands is sharply increased with the shift of their maxima to 447 and 828 nm, respectively (Fig. 8, curve 3). As is known [33], the shape, position, and size of silver and silica nanoparticles affect the shape and position of SPR band. The observed changes in the absorption spectrum are explained by higher amounts of silver nanoparticles formed under sunlight action. Two broad absorption bands in the spectrum of 02Ag-F (Fig. 7, curve 3) sample can be explained by the formation of silver nanoparticles of different size and shapes after daylight exposure. The appearance of an SPR band in the region of 725 nm (AgNPs) changes the view of the spectrum of 02Ag02Cu-F (Fig. 8) sample and leads to a shift in the absorption band maximum of copper oxide.

It must be pointed out that the SPR band of AgNPs disappears after UV irradiation for 30 min, whereas the absorption band of CuO remains almost unchangeable (Fig. 8, solid lines) taking into account that copper oxide on the fumed silica surface with the content of 0.2 mmol/g SiO_2 is XRD amorphous as previously established by us [26]. In the case of all samples irradiated by UV light in air, the disappearance of SPR band can be caused by partial or complete oxidation of Ag^0 to Ag^+.

Significant visible changes in the colour of the powders after UV light action are not observed (Fig. 9c, d) due to the possible oxidation of Ag^0 to Ag^+ as shown by the SPR band disappearance. However, the daylight exposure on the powders for 10 days led to visual their darkening (Fig. 9e, f).

The synthesized samples before and after sunlight exposure for 10 days were analysed by XRD method. The obtained data show the appearance of only an

Fig. 9 Images of samples: 02Ag-F (upper row) and 02Ag02Cu-F (bottom row) before irradiation (**a**, **b**), after under UV light for 60 min (**c**, **d**), and after sunlight exposure for 10 days (**e**, **f**)

amorphous halo of fumed silica. After additional scanning of the area of the most intensive XRD lines of crystallized silver with a step of 0.02°, a weak peak was revealed indicating the presence of an insignificant quantity of nanocrystalline silver for the samples subjected to daylight (Fig. 10).

The observed silver transformations in nanocomposites after sunlight exposure can be explained by the processes of coalescence induced by light that are followed
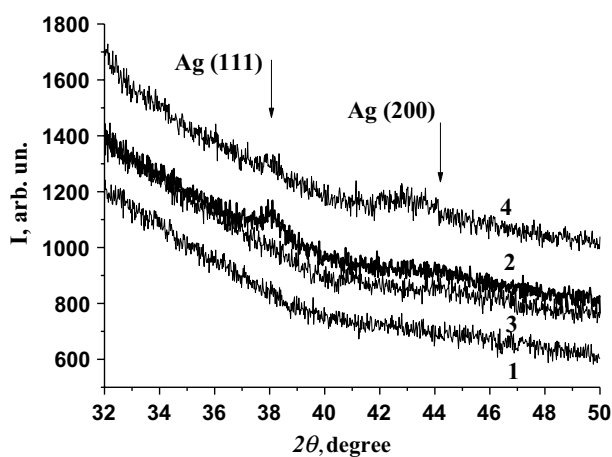

Fig. 10 XRD patterns of 02Ag-F (1, 2) and 02Ag02Cu-F (3, 4) samples before (1, 3), and after daylight exposure for 10 days (2, 4)

by silver particles growth and changes in their form. Callegari et al. showed the way of the size and shape of colloidal particles change upon irradiation with light of different wavelengths [42]. Nonetheless, the formation of Ag$_2$O crystallites in the 1Ag-F sample (with a high content of silver) under the same conditions is observed (Fig. 6). For 02Ag-F and 02Ag02Cu-F samples, the opposite transformations were observed under UV radiation resulting in the intensity decrease of SPR band (Figs. 8 and 9), which can be caused by the oxidation of Ag^0 and the formation of Ag$_2$O nanoparticles.

The photoinduced transformation of silver ions in aqueous solution under UV irradiation at 254 nm through reduction by water molecules as a result of the electron-transfer to the electronically excited state of Ag$^+$ to form Ag^0 is reported [43].

$$Ag^+ + H_2O + h\nu \rightarrow Ag^\circ + H^+ + HO^\cdot \tag{1.2}$$
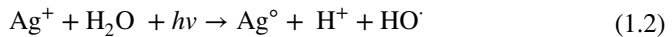
This reaction can also occur in our systems. It is assumed that the rate of reaction of photoinduced oxidation of Ag^0 and the formation of amorphous silver oxides is higher than the rate of reduction reaction in the presence of adsorbed water. Additionally, mechanochemical activation of dispersive systems is followed by the change in structural and adsorption characteristics of materials that can also affect the chemical transformations in the surface layers of dispersive silica [44, 45].

All samples of this series after UV/sunlight irradiation were tested for biocidal activity. The results of statistical processing of measurement of growth inhibition zones are given in Table 3.

It is known that the nanostructures based on compounds of silver and copper improve the antifungal protection of materials [27, 46, 47]. However, a significant improvement of antimicrobial activity in the presence of CuO has not been established in this study (Table 3). It must be noted that UV or sunlight exposure leads to the increase in the antimicrobial activity of composites contained only silver as well

Table 3 Growth delay zones (in mm) of microorganisms in the presence of composites after daylight exposure for 10 days and UV irradiation for 30–120 min

Light sources	Samples	*Escherichia coli*	*Candida albicans*	*Staphylococcus aureus*	*Bacillus subtilis*
Without irradiation	02Ag-F	22.25 ± 0.63	20.50 ± 0.50	28.50 ± 1.55	24.25 ± 0.48
	02Ag02Cu-F	20.50 ± 0.29	22.50 ± 0.29	28.00 ± 0.58	24.25 ± 0.48
Sunlight 10 days	02Ag-F	25.50 ± 0.50	25.50 ± 0.65	28.50 ± 0.29	25.25 ± 0.48
	02Ag02Cu-F	22.25 ± 0.75	23.75 ± 0.75	28.00 ± 0.91	24.75 ± 1.31
UV 30′	02Ag-F	23.00 ± 1.47	22.50 ± 0.50	27.25 ± 0.95	24.00 ± 0.41
	02Ag02Cu-F	20.50 ± 0.65	24.25 ± 0.48	27.50 ± 0.65	25.50 ± 1.44
UV 60′	02Ag-F	35.75 ± 1.18	23.75 ± 0.85	28.50 ± 1.04	29.50 ± 1.19
	02Ag02Cu-F	31.50 ± 1.85	25.25 ± 0.48	29.75 ± 0.85	27.50 ± 1.19
UV 90′	02Ag-F	30.50 ± 0.50	33.00 ± 0.91	24.00 ± 0.41	36.50 ± 0.29
	02Ag02Cu-F	27.00 ± 0.91	28.75 ± 0.63	26.75 ± 0.63	32.75 ± 1.03
UV 120′	02Ag-F	36.00 ± 0.82	35.25 ± 0.63	25.75 ± 1.03	37.25 ± 1.03
	02Ag02Cu-F	32.50 ± 1.04	30.00 ± 0.71	28.75 ± 1.11	34.75 ± 1.11

as silver and copper. However, a statistically reliable increase in the activity of composite contained silver and copper was not observed in comparison with the sample containing only silver under the equal conditions of photoactivation. An insignificant increase in the bioactivity after UV irradiation can be caused by the formation of silver oxides, which can cause the formation of Ag^+ in contact with the culture fluid of the nutrient medium. The highest antimicrobial activity of 02Ag02Cu-P sample in the polymer may be associated with the high content of silver (nanoparticles and ions) (Table 2).

Conclusion

Mechanochemical activation is an effective approach to synthesize Ag and AgCu containing silica nanocomposites that exhibit antimicrobial properties and provide the similar properties for filled polymeric materials. During thermal destruction of silver nitrate and ammonium complexes of metal in the silica matrix, amorphous and nanosized structures of silver oxides and metallic Ag nanocrystallites are formed. As shown by absorption spectra of the AgCu contained nanocomposites, the SPR band in the region of 400–420 nm and the broad absorption in the range of 760–900 nm point on the formation of AgNPs of the different sizes and shapes as well as copper species. The growth of silver nanocrystallites in nanocomposites subjected to sunlight exposure takes place, which is detected by the increase of the SPR band as well as its shift to the longer wavelengths of the spectra. It is shown that UV irradiation causes possible oxidation of Ag^0 to Ag^+ ions as an intensity decrease in the surface plasmon resonance band is observed. Such transformations of silver compounds ($Ag^+ \leftrightarrow Ag^0$) have no influence on the biocidal activity of nanocomposites that can be used as antimicrobial fillers of polymer materials.

References

1. A. Kahru, H-Ch. Dubourguier, Toxicology **269**, 105 (2010)
2. Z. Wang, Y.-H. Lee, B. Wu, A. Horst, Y. Kang, Y.J. Tang, D.-R. Chen, Chemosphere **80**, 525 (2010)
3. P.A. Patil, B.R. Bhutkar, Y.D. Dange, S.V. Kharat, J. Nanomed. Nanotechnol. **7**, 1 (2016)
4. B. Nowack, H.F. Krug, M. Height, Environ. Sci. Technol. **45**, 1177 (2011)
5. M. Rai, A. Yadav, A. Gade, Biotechnol. Adv. **27**, 76 (2009)
6. R.P. Allaker, K. Memarzadeh, Int. J. Antimicrob. Agents **43**, 95 (2014)
7. M. Moritz, M. Geszke-Moritz, Chem. Eng. J. **228**, 596 (2013)
8. N.Y. Hebalkar, S. Acharya, T.N. Rao, J. Colloid Interface Sci. **364**, 24 (2011)
9. A. Mukhopadhyay, S. Basak, J.K. Das, S.K. Medda, K. Chattopadhyay, G. De, ACS Appl. Mater. Interface **2**, 2540 (2010)
10. X.-H. Guo, J.-Q. Ma, H.-G. Ge, J. Phys. Chem. Solids **74**, 784 (2013)
11. L. Feng, W. Shen, H. Feng, A. Lei, Zh Liu, Ceram. Int. **40**, 6963 (2014)
12. A. Eremenko, N. Smirnova, Iu Gnatiuk, O. Linnik, N. Vityuk, Iu Mukha, A. Korduban, in *Nanocomposites and Polymers with Analytical Methods*, ed. by J. Cuppoletti (InTech, Croatia, 2011), p. 404
13. A.M. Eremenko, N.P. Smirnova, I.P. Mukha, H.R. Yashan, Theor. Exp. Chem. **46**, 65 (2010)
14. T.M. Tolaymat, A.M. El Badawy, A. Genaidy, K.G. Scheckel, T.P. Luxton, M. Suidan, Sci. Total Environ. **408**, 999 (2010)

15. Sh Li, T. Zhang, Zh Zhu, N. Gao, Q.-H. Xu, RSC Adv. **6**, 58566 (2016)
16. M. Nishioka, M. Miyakawa, H. Kataoka, H. Koda, K. Sato, T.M. Suzuki, Chem. Lett. **40**, 1204 (2011)
17. M. Priebe, J. Widmer, N.S. Löwa, S.-L. Abram, I. Mottas, A.-K. Woischnig, P.S. Brunetto, N. Khanna, C. Bourquin, K.M. Fromm, Nanomed. Nanotech. Biol. Med. **13**(1), 11 (2017)
18. J.C. Flores, V. Torres, M. Popa, D. Crespo, J.M. Calderón-Moreno, Colloids Surf. A **330**, 86 (2008)
19. R. Qin, G. Li, L. Pan, Q. Han, Y. Sun, Q. He, J. Nanosci. Nanotechnol. **17**, 2305 (2017)
20. K. Woo, Y.-S. Ko, S.-H. Park, J.-H. Lee, J. Hwang, Adv. Mater.: TechConnect Briefs **1**, 253 (2016)
21. ChY Kim, S-Ch. Yi, J. Ceram. Process. Res. **10**, 462 (2009)
22. S.-H. Min, J.-H. Yang, J.Y. Kim, Y.-U. Kwon, Microporous Mesoporous Mater. **128**, 19 (2010)
23. J. Ma, J. Zou, L. Li, Ch. Yao, T. Zhang, D. Li, Appl. Catal. B **134–135**, 1 (2013)
24. X. Jiang, Sh Chen, C. Mao, Colloids Surf. A **320**, 104 (2008)
25. M. Huang, X. Yang, J. Zhao, Q. Wang, Res. Chem. Intermed. **40**, 1957 (2014)
26. V.M. Bogatyrov, O.I. Oranska, M.V. Galaburda, I.I. Gerashchenko, T.P. Osolodchenko, V.I. Yusyp-chuk, CPTS **7**, 44 (2016)
27. V.M. Bogatyrov, M.V. Galaburda, O.M. Zaichenko, K.S. Tsyganenko, Ya.I. Savchuk, Surface **7**, 119 (2015)
28. T.A. Kotelnikova, Russ. J. Phys. Chem. A **91**, 1301 (2017)
29. H. Granbohm, Ju Larismaa, S. Ali, L.-S. Johansson, S.-P. Hannula, Materials **11**, 80 (2018).
30. H.-L. Liu, ShA Dai, K.-Y. Fu, Sh-H Hsu, Int. J. Nanomed. **5**, 1017 (2010)
31. T. Rudenchyk, R. Rozhnova, N. Galatenko, Adv. Biochem. **5**, 73 (2017)
32. M. Balouiri, M. Sadiki, S.K. Ibnsouda, J. Pharm. Anal. **6**, 71 (2016)
33. M. Zhu, G. Qian, G. Ding, Zh Wang, M. Wang, Mater. Chem. Phys. **96**, 489 (2006)
34. O.A. Yeshchenko, I.M. Dmitruk, A.A. Alexeenko, A.V. Kotko, J. Verdal, A.O. Pinchuk, Ukr. J. Phys. **57**, 266 (2012)
35. K. Nischala, T.N. Rao, N. Hebalkar, Colloids Surf. B Biointerfaces **82**, 203 (2011)
36. S.A. Kong, H. Wang, X. Yang, Ya. Hou, Y. Shan, Microporous Mesoporous Mater. **118**, 348 (2009)
37. X. Jiang, H. Deng, Colloids Surf. A: Physicochem. Eng. Asp. **330**, 180 (2008)
38. R. Zeng, M.Z. Rong, M.Q. Zhang, HCh. Liang, H.M. Zeng, J. Mater. Sci. Lett. **20**, 1473 (2001)
39. K. Otto, I.O. Acik, M. Krunks, K. Tõnsuaadu, A. Mere, J. Therm. Anal. Calorim. **118**, 1065 (2014)
40. G.A. Sotiriou, A. Meyer, J.T.N. Knijnenburg, S. Panke, S.E. Pratsinis, Langmuir **28**, 15929 (2012)
41. P.E. Cardoso-Avila, J.L. Pichardo-Molina, C.M. Krishna, R. Castro-Beltran, J. Nanopart Res. **17**, 160 (2015).
42. A. Callegari, D. Tonti, M. Chergui, Nano Lett. **3**, 1565 (2003)
43. N.L. Pacioni, C.D. Borsarelli, V. Rey, A.V. Veglia, in *Silver Nanoparticle Applications in the Fabrication and Design of Medical and Biosensing Devices*, ed. by E.I. Devices, M. Alarcon, K.I.Udekwu Griffith (Springer, Basel, 2015), p. 13
44. V.M. Gun'ko, E.F. Voronin, L.V. Nosach, V.V. Turov, Z. Wang, A.P. Vasilenko, R. Leboda, J. Skubiszewska-Zięba, W. Janusz, S.V. Mikhalovsky, J. Colloid, Interface Sci. **355**, 300 (2011)
45. R. Rattanakam, S. Supothina, Res. Chem. Intermed. **35**, 263 (2009)
46. M. Jalbrzykowski, K. Leszczynska, S. Obidzinski, Ł. Minarowski, M. Laabs, Agric. Eng. **22**, 49 (2018).
47. V.M. Bogatyrov, O.I. Oranska, M.V. Galaburda, L.O. Yakovenko, K.S. Tsyganenko, Ya.I. Savchuk, O.M. Zaichenko, Surface **8**, 259 (2016)